Eur. J. Mineral.
2015, **27**, 617–626
Published online 22 June 2015

Low-temperature chlorite geothermometry: a graphical representation based on a T–R^{2+}–Si diagram

FRANCK BOURDELLE[1,2,*] and MICHEL CATHELINEAU[2]

[1] LGCgE, Université Lille 1, 59655 Villeneuve d'Ascq, France
[2] CNRS, CREGU, GeoRessources Laboratory, Université de Lorraine, 54506 Vandœuvre-lès-Nancy, France
*Corresponding author, e-mail: franck.bourdelle@univ-lille1.fr

Abstract: The chlorites are good indicators of rock history because their wide compositional variations are sensitive to the formation conditions, like pressure (P), temperature (T), redox state, fluid composition. Accordingly, many geothermometers based on their composition, either empirically or thermodynamically, have been proposed during the last 30 years, especially in low-temperature contexts ($T < 350$°C). This paper presents a graphical tool that considerably facilitates the use of two of the most recent chlorite thermometers for low- and very-low-T chlorites. The temperature–composition relationships for low-T chlorites are represented in T–R^{2+}–Si diagrams, allowing chlorite compositions to be predicted as a function of temperature or, conversely, temperature to be estimated from compositional fields of natural chlorites. This graphical projection is based on a comparison of the parameters (ideal chlorite compositions and calculated T) predicted by geothermometers with analyses of natural chlorites for which independent T estimates are available over a range of geological environments. The new T–R^{2+}–Si diagram provides a practical tool for thermometric purposes in the applicability range of the considered models, in particular for diagenesis and low-grade metamorphism.

Key-words: chlorite; geothermometry; diagenesis; low-grade metamorphism; solid solution model.

1. Introduction

Chlorites are relevant indicators of rock history because their wide compositional variations are sensitive to the formation conditions, *i.e*. pressure (P), temperature (T), the redox conditions, as well as to bulk-rock and fluid composition. Therefore, chlorite composition is the basis of many geothermometers that are commonly applied in very diverse contexts (*e.g*. Inoue *et al*., 2010; Kameda *et al*., 2011, 2012; Ganne *et al*., 2012; Grosch *et al*., 2012).

Three approaches have been used to establish such geothermometers. The first consists of empirical calibrations, which were proposed to directly link the chlorite composition to the temperature. Most of these calibrations relied on variations in the tetrahedral Al content (Cathelineau & Nieva, 1985; Kranidiotis & McLean, 1987; Cathelineau, 1988; Hillier & Velde, 1991; Jowett, 1991; Zang & Fyfe, 1995), mirrored by Si counter-variation. However, these methods failed to obtain accurate estimates in several instances (*e.g*. de Caritat *et al*., 1993; Bourdelle *et al*., 2013a), because they cannot take into account the three main cationic substitutions occurring in chlorites, *i.e*., ferromagnesian (Fe^{2+} = Mg), Tschermak ($Al^{IV}Al^{VI}$ = Si[Mg, Fe^{2+}]) and di/trioctahedral (3[Mg, Fe^{2+}] = □ + $2Al^{VI}$; where □ represents an octahedral vacancy). Consequently, these empirical methods can only be applied to a restricted range of chlorite compositions, *i.e*. close to those used to define the geothermometer relationship. The second approach is based on thermodynamic databases (*e.g*., Vidal *et al*., 2001, 2005, 2006; Lanari *et al*., 2014) and takes into account the non-ideality of the solid solution and the P effect. This thermodynamic approach is the most rigorous; however, it requires complex calculations and hinges on the availability of solid-solution models and end-member thermodynamic data, which limits the range of P-T-X domains of application. For instance, the most recent thermodynamic model proposed for chlorite thermometry, *e.g*. Lanari *et al*. (2014), is inappropriate for most low-T chlorites because its choice of end-members cannot account for the Si-rich chlorites (Si > 3 atoms per formula unit, apfu), which occur in most sedimentary or hydrothermal contexts.

The third approach, which can be referred to as semi-empirical, considers the chlorite + quartz equilibrium and uses ratios of end-member activities to link chlorite composition to temperature through the equilibrium constant K (Walshe, 1986; Inoue *et al*., 2009; Bourdelle *et al*., 2013b; Lanari *et al*., 2014). Although these thermometers require several assumptions to be applicable (since they do not consider explicitly the contributions of non-ideality, P, water activity, *etc*.), they are easy to use, they circumvent the issue of the bulk composition and they perform well in

0935-1221/15/0027-2467 $ 4.50
DOI: 10.1127/ejm/2015/0027-2467

diagenetic to low-grade metamorphic contexts (*e.g*. Inoue *et al*., 2010; Bourdelle *et al*., 2013b; Harbi *et al*., 2014), in particular in the *T*-range where Si-rich chlorites are observed (except for the semi-empirical equations of Lanari *et al*. (2014), which exclude Si $>$ 3 apfu chlorites). Moreover, the objections raised above can be ruled out for low-*T* low-*P* conditions, especially in hydrothermal systems where water activity does not vary significantly. Therefore, and contrary to empirical equations, the approach preferred by Inoue *et al*. (2009) and Bourdelle *et al*. (2013b) predicts that one chlorite composition corresponds to one temperature of formation, but that at any fixed temperature a range of equilibrium chlorite composition exists and can be calculated.

The incentive for the present paper was the request by several users of Bourdelle *et al*. (2013b) thermometer for a more user-friendly formulation. Therefore, we propose here to transpose the predictions of the recent Inoue *et al*. (2009) and Bourdelle *et al*. (2013b) models into an easy-to-use graphical tool, which provides a clear visual explanation of the changes occurring in chlorite composition as a function of temperature. The focus is on low- and very-low-*P*-*T* chlorites, *i.e.* $T < 350$°C and $P < 3$–4 kbar, conditions that are of central interest in, *e.g*., exploration geology. The keys of the new proposed diagrams are given in the second part of the paper through comparison of several published data sets (*i.e*. composition/*P*-*T* conditions for a given natural chlorite) to the calculated compositions at given *T*.

2. Sources and selection of chlorite analyses

In order to test the suitability of geothermometers and their graphical projections across a wide spectrum of *P*-*T* conditions and geological environments, published data concerning low-*T* chlorite compositions were screened. The specifications governing the selection of the data were as follows:

- The data must constitute sets of chlorite analyses: each set must refer to a defined geological field while covering a wide compositional range or a large temperature window. This is why several studies (such as Beaufort *et al*., 1992, or Xie *et al*., 1997), although they provide suitable chlorite analyses, are used only in the second part of the present paper.
- The data must consist of a detailed quantitative analysis of chlorites by electron microprobe (EMP) or transmission electron microscope equipped with energy-dispersive X-ray spectroscopy systems (TEM-EDX), which should be available along with temperature and pressure data in the range of 50–350°C and below 4 kbar (application domain of the Bourdelle *et al*. (2013b) model). The temperature data were used as published when their estimates were given with a sufficient level of confidence (*i.e*. use of independent temperature measurements or convergence of several thermometric methods). The pressure data refer to the author's estimates whenever possible and to the indications of geological context ensuring that the formation pressure was less than 4 kbar. In cases of uncertainty or insufficient level of confidence regarding the *P*–*T* data, the analyses were discarded; for instance, some important studies such as Jowett (1991); Zang & Fyfe (1995) and Inoue *et al*. (2009) had to be discarded because pressure estimates were not available or because temperature data were not assigned to specific chlorite compositions.
- All published data used here are considered as referring to authigenic chlorites. Detrital materials were discarded, as in the study by Rahn *et al*. (1994), where authigenic and detrital compositions were identified.
- Only quartz–chlorite assemblages were considered.
- Contaminated analyses were rejected ($K_2O + Na_2O + CaO < 1$ wt % as general criterion for both EMP and AEM analysis) as well as those that could not be expressed as a linear combination of end-members.

3. Formulation of low-*T* chlorite geothermometers

3.1. Model calculation

The available geothermometers based on the chlorite + quartz equilibrium use the equilibrium condition for any balanced reaction involving *j* end-members, which can be expressed as:

$$\Delta G_r^0 + R.T.\ln K = 0 \quad (1)$$

where ΔG_r^0 is the Gibbs free energy of reaction, *R* is the gas constant and *K* is the chlorite + quartz equilibrium constant. This equilibrium constant can be written as:

$$K = \prod_j \left(a_{\text{ideal}}\gamma_m\right)_j^{v_j} \quad (2)$$

with v_j as the stoichiometric reaction coefficient of end-member *j*, a_{ideal} the ideal part of the end-member activity and γ_m the activity coefficient.

Each thermodynamic model has its own limits (*e.g*. considering non-ideality or not in Eq. (2), based on a thermodynamic database or on a ratio of end-member activities) and its own application domain. Therefore, the models of Vidal *et al*. (2001, 2005, 2006) and Lanari *et al*. (2014), due to their choice of end-members excluding high-Si chlorites, are inappropriate for low-T contexts (Fig. 1) but give excellent results and perform well on high-*T* chlorites. Conversely, the model of Walshe (1986) excludes many Si-poor chlorite compositions (Fig. 1). In turn, the models of Inoue *et al*. (2009) and Bourdelle *et al*. (2013b) are suitable for low-*T* chlorites, but neglect pressure and non-ideal contributions.

In the present study focused on low-*T* chlorites (50–350°C), only the models of Inoue *et al*. (2009) and Bourdelle *et al*. (2013b) are considered. These two thermometers are ideal models based on end-member activity ratios and directly link the temperature to the *K* equilibrium constant as:

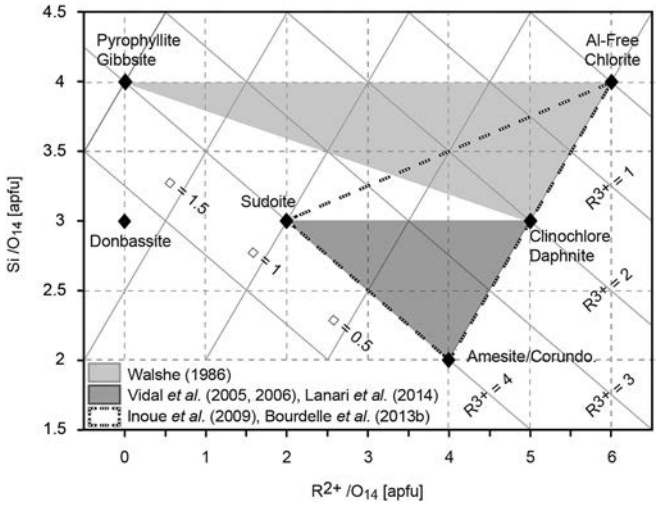

Fig. 1. Projection field (R^{2+}–Si diagram) for chlorite compositions after Wiewióra & Weiss (1990). R^{2+} refers to divalent cations (Fe^{2+} and Mg^{2+}), R^{3+} to trivalent cations (Al^{3+}, Fe^{3+}) and □ to vacancies. Values are given in atoms per half-formula unit (apfu) with a 14 oxygen basis. Several end-members are indicated and the compositional spaces defined by the models of Walshe (1986); Vidal *et al*. (2001, 2005, 2006), Inoue *et al*. (2009) and Bourdelle *et al*. (2013b) are outlined.

$$\log K = \frac{-\Delta G^0_r}{2.303(R.T)} = \frac{A}{T} + B \quad (3)$$

where A and B are constants. The two semi-empirical models neglect the effect of pressure, $B = \Delta S \div (2.303 \times R)$, given the ΔCp approximation. This assumption is especially justified in low-*T*/low-*P* contexts. Inoue *et al*. (2009) chose the magnesian end-members of Al-free Mg-chlorite (also denoted chlorite S), of 'corundophilite' and of sudoite, and the ferrous end-member of chamosite (Fig. 1), while Bourdelle *et al*. (2013b) selected the magnesian and ferrous end-members of Al-free chlorite, amesite (similar to 'corundophilite') and sudoite (Fig. 1). The two thermometers differ by their cationic site repartition model: Inoue *et al*. (2009) assume a random mixing of octahedral cations, based on the fact that Fe-rich chlorites commonly are the Ib polytype for which details of the crystal structure are not clearly established, whereas Bourdelle *et al*. (2013b) chose an ordered cationic site repartition model (*cf.* Appendices S1 and S2, freely available online, linked to this article on the GSW website of the journal, HYPERLINK http://eurjmin.geoscienceworld.org/http://eurjmin.geoscienceworld.org/), following the recommendations of Vidal *et al*. (2001) and Bailey (1988) for di-trioctahedral chlorites.

According to the chlorite + quartz equilibrium, the two models are based on the following reaction:

$$\text{Al-free Mg-chlorite} + 3\ \text{Mg-sudoite} = 3\ \text{Mg-amesite} + 7\ \text{Quartz} + 4H_2O \quad (4)$$

The thermometers were calibrated assuming $aH_2O = aSiO_2 = 1$. The values of H_2O activity in the fluid are unknown but the assumption $aH_2O = 1$ is reasonable under diagenetic to low-grade metamorphic conditions (Inoue *et al*., 2009; Lanari *et al*., 2014), while the assumption $aSiO_2 = 1$ is justified in the case of quartz-bearing rocks.

Considering the previous reaction and assumptions, the log K value of the chlorite + quartz equilibrium is independent of the Fe/(Fe + Mg) ratio. Indeed, in the case of Inoue, the contribution of the Mg molar fraction (X_{Mg}) in the end-member activities calculation is $(X_{Mg,oct})^6$, $(X_{Mg,oct})^2$ and $(X_{Mg,oct})^4$ for Al-free chlorite, sudoite and 'corundophilite', respectively (Inoue *et al*., 2009; Appendix S1). According to the reaction stoichiometric coefficients, the total contribution of Mg in the K calculation becomes $(X_{Mg,oct})^{12}$ on each side of the equilibrium, implying that log K is independent of $X_{Mg,oct}$ (Eq. 5):

$$\log K = \frac{a^3_{Mg-Am} \cdot a_{Qz} \cdot a_{H_2O}}{a^3_{Mg-Sud} \cdot a_{Mg-ChlS}} = \frac{\left(45.563 \times (X_{Mg})^4 (X_{Al,tet})^2 (X_{Al,oct})^2\right)^3}{(X_{Mg})^6 \times (X_{Si})^2 \times \left(1728 \times (X_{Mg})^2 \times (X_{Al,oct})^3 \times (X_{[]}) \times (X_{Si}) \times (X_{Al,tet})\right)^3} \quad (5)$$

In the same way, in Bourdelle's model involving three magnesian and three ferrous end-members, the log K depends on Si and Al contents, and on the Mg_{M2}/Mg_{M1} ratio. However, this ratio is constant regardless of XMg (due to its dependence on the Al cationic repartition) for defined contents of Si, Al and R^{2+}, making the log K of the chlorite + quartz equilibrium equal in both the magnesian and ferrous systems for each specific composition.

The calibrated thermometer of Bourdelle *et al*. (2013b), following Eq. 3 and (4), was expressed by a linear equation:

$$\log K = -\frac{9400}{T(\mathrm{K})} + 23.40 \quad (6)$$

Inoue *et al*. (2009) indicate that the upper application limit of their thermometer is 250°C, and prefer a quadratic formalism as the main equation:

$$T(\mathrm{K}) = \frac{1}{0.00293 - 0.000513 \log K + 0.00003904 (\log K)^2} \quad (7)$$

but express it also in a linear form (Eq. 3):

$$T(\mathrm{K}) = \frac{1}{0.00264 - 0.0002897 \log K} \quad (8)$$

Concerning ferric iron, Inoue *et al*. (2009) model takes it into account while Bourdelle *et al*.'s (2013b) model ignores it.

3.2. Graphical representation of the geothermometers

The relationships between chlorite composition and temperature of formation have been represented through isotherms in a R^{2+}–Si diagram (Wiewióra & Weiss, 1990), which is a useful plot to display R^{2+}-Si-Al-vacancies

relationships. From this representation, all the compositions in equilibrium at a given temperature project on the same graphic isotherm. As Inoue *et al*. (2009) and Bourdelle *et al*. (2013b) models provide identical temperature estimates in the magnesian and the ferrous systems, any given point on an isotherm represents chlorites having the same R^{2+} content (*i.e*., $Fe^{2+}+Mg^{2+}$; all iron is considered as ferrous, see section 3.3.3) but the whole range of XFe ratios ($XFe = Fe^{2+}/[Fe^{2+}+Mg]$), between 0 and 1.

Several standard chemical compositions covering the Al-free chlorite–amesite–sudoite space were used to simulate *T* calculations, with Si contents ranging from 2 to 4 apfu on a 14 oxygen basis. Considering the end-members used in Inoue *et al*. (2009) and Bourdelle *et al*. (2013b) models, the focus was on the bottom of the R^{2+}–Si diagram, where $R^{2+} > 2$ apfu (red area in Fig. 1). According to the electroneutrality principle, the R^{3+} content (trivalent cations), without distinguishing between Al and Fe^{3+}, was calculated as follows:

$$R^{3+} = \frac{28 - 2R^{2+} - 4Si}{3} \quad (9)$$

From this formalism, the chlorite compositions are considered as ideal, *i.e*., devoid of tetrahedral Ti, octahedral Mn or any K, Na, Ca contamination.

3.3. Assumptions and model applicability

Beyond the divergence between empirical, semi-empirical and thermodynamic models, two main paths can be followed to obtain thermometric perspectives. The first consists in simplifying the geothermometry while conserving a fundamental thermodynamic basis. The second is to refine the existing thermodynamic and solid-solution parameters to develop models that can be implemented in the existing thermodynamic database. The thermodynamic approach is admittedly more rigorous; however, the semi-empirical approach makes sense when the main goal is to easily estimate the temperature, in particular when the investigated domain presents a lack of thermodynamic data, as is the case for very low-*T* chlorites. The condition of validation is to make the simplifications identifiable and to quantitatively evaluate their impact on *T* estimates. The validity of these trade-offs is proven by the success of semi-empirical thermometers in applications to various geological contexts (*e.g*. Inoue *et al*., 2010; Bourdelle *et al*., 2013b; Yoneda & Mokko, 2013; Harbi *et al*., 2014). The other simplifications that justify a semi-empirical approach are summarized in the following sections.

*3.3.1. Choice of ideal model for low-*T *chlorites*

The semi-empirical $T = f(K)$ calibration requires to neglect the non-ideal contribution of site mixing. As shown by Bourdelle *et al*. (2013b), the assumption of ideal mixing is tenable if one verifies that (1) for a given chlorite composition, the contribution of non-ideality varies linearly with $1/T$, and (2) at given *T*, the variation in the non-ideal contribution with chlorite composition is small, so that the net effect of non-ideality in *T* is grossly linear and so makes an empirical calibration possible.

The first point is verified by the mathematical expression of non-ideality, in which the non-ideal contribution in the log/ln *K* calculation is linear in $1/T$ for a fixed composition. The second point was checked by Bourdelle (2011) and Bourdelle *et al*. (2013b), who tested the semi-empirical approach for various chlorite compositions and *P-T* conditions in varying the $X_{Si,T2}$, XMg (ratio) and $X_{\square}$, and who showed that the variation in the non-ideal contribution with composition (over the classical range of diagenetic chlorites) is sufficiently small for the linearity of log/ln *K* in $1/T$ to be grossly preserved, especially in the temperature and compositional domains investigated here (*i.e*., 100–350°C; $2.7 < Si < 3.6$ apfu). This justifies calibration on a linear basis and, effectively, any effect of non-ideality is implicitly taken into account in the thermometer equations.

3.3.2. Choice of models without Fe-Mg exchange

The two models used here for graphical projections provide identical temperature estimates in the magnesian and ferrous systems. This is not an assumption but the result of the semi-empirical calibration, of the choice of end-members and of the formalism of the chlorite + quartz equilibrium. Indeed, the thermometer equation is based on equilibrium (4) which does not take into account the ferromagnesian exchange. As explained in section 3.1, the log *K* is independent of $X_{Mg,oct}$, *i.e*., the Fe/(Fe + Mg) ratio does not play a role in the temperature estimation.

Vidal *et al*. (2005) explained that experimental data obtained in the MASH and FASH systems are inconsistent with the assumptions of identical Fe/Mg on-site energetics or identical Fe-Al/Mg-Al interaction energetics. The impact of Fe-Mg exchange on the *T*–composition relationship is especially true in high-*T* contexts. In low-*T* domains, the main exchange linked to the temperature variation remains the $Si_{-1}\square_{-1}R_2^{2+}$ exchange vector (or close to it, see section 4.1 and Fig. 3), independent of the nature of the R^{2+} cations. Therefore, even if semi-empirical thermometers do not explicitly account for ferromagnesian exchanges and on-site interactions, they can give suitable results through the main cationic substitution (i) in low-*T* contexts and (ii) in the compositional range of low-*T* chlorites ($1.5 < R^{3+} < 3.5$ apfu).

*3.3.3. Fe^{3+} in low-*T *chlorites*

Consideration of iron valence in chlorite thermometry is a long debate. First of all, the evaluation of Fe^{3+} content is rarely issued from direct analysis because the *in situ* nanoanalysis of the pristine Fe^{3+}/Fe^{2+} ratio of chlorite remains an analytical challenge (TEM-EELS, STXM-XANES), and can be affected by oxidation during preparation (thin sections, crushing).

Vidal *et al*. (2001) propose a reliable model for high-*T* chlorites which does not consider Fe^{3+}, but Vidal *et al*.

(2005, 2006) show the impact of Fe^{3+} content in thermometric predictions at lower *T*. Inoue *et al*. (2009) established a semi-empirical model specially adapted for low-*T* chlorites, but requiring that the Fe^{2+}/Fe^{3+} ratio is known. Bourdelle *et al*. (2013b) proposed a new low-*T* chlorite thermometer, considering all iron as Fe^{2+}. Bourdelle *et al*. (2013b) justify this approach by the fact that accounting for Fe^{3+} in the structural formula recalculation on a fixed oxygen basis arithmetically reduces the number of cations, and implies an increase of octahedral vacancies, which in turn links indirectly Fe^{3+} content and temperature in any thermometric formulation. This effect of the non-consideration of Fe^{3+} has a subordinate role because temperature estimates are controlled in first place by the Tschermak and di-trioctahedral substitutions (compare Figs 6(a) and (b) in Inoue *et al*., 2009). In order to evaluate the impact of considering the estimate of the Fe^{3+}/Fe^{2+}ratio, we compare the results obtained with the thermometers of Bourdelle and Inoue for a defined low-*T* chlorite composition and by varying the iron content (XFe) and the $Fe^{3+}/(Fe^{3+}+Fe^{2+})$ ratio. The results are presented in Fig. 2, considering that the convergence of the two thermometers is reached when the difference between their predictions is less than 20°C. Thus, for a starting composition of Si = 3.1 and R^{2+} = 4.17 apfu for which Bourdelle's thermometer yields *T* = 127°C, the convergence is reached regardless of the XFe or the $Fe^{3+}/(Fe^{3+}+Fe^{2+})$ ratio. As an example, for a high $Fe^{3+}/(Fe^{3+}+Fe^{2+})$ ratio of 0.4, Inoue's thermometer predicts 116°C if all R^{2+} is Fe^{2+}, and 146°C if all R^{2+} is Mg, *i.e.* within 11 and 19°C of Bourdelle's prediction, respectively. The lower the temperature, the lower is the impact of Fe^{3+} on the convergence of the two models. Therefore, a calibration based on a Fe^{2+}-Fe^{3+} mix model should lead to higher precision, but a calibration based on a pure-Fe^{2+} model is a good trade-off of practicability and simplicity (no Fe^{3+} content required) while giving suitable results. Moreover, Bourdelle *et al*. (2013b) and Bourdelle *et al*. (2013c), on the basis of Mössbauer, X-ray photoelectron spectroscopy and X-ray absorption near-edge spectroscopy data, showed the convergence of the temperatures estimated using the two models despite the difference in accounting for Fe^{3+}.

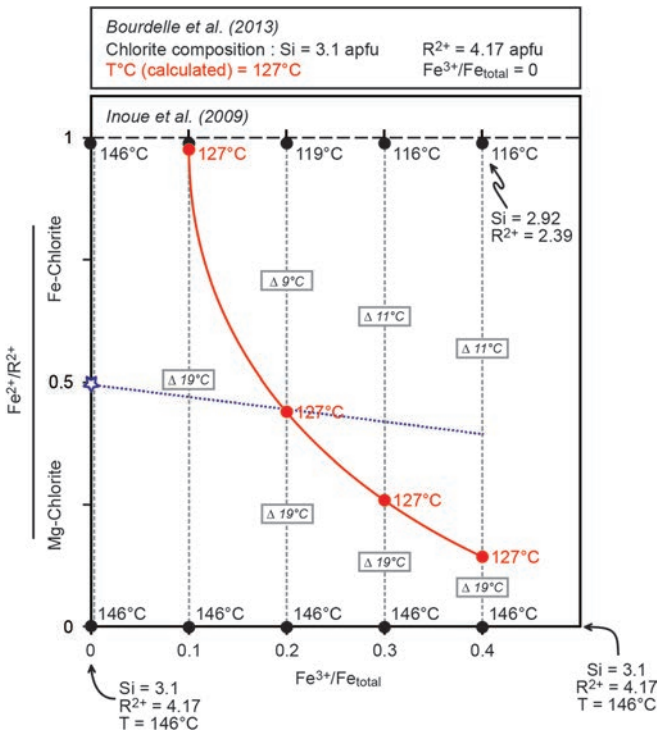

Fig. 2. Predictions of Bourdelle and Inoue thermometers as a function of Fe^{2+}/R^{2+} and $Fe^{3+}/(Fe^{3+}+Fe^{2+})$ ratios. From a starting chlorite composition with fixed Si, Al and R^{2+} contents and Fe^{3+} = 0, the temperature was estimated with Inoue's model by varying XFe and $Fe^{3+}/(Fe^{3+}+Fe^{2+})$. The convergence between the two thermometers is considered reached when the difference is lower than 20°C. No Fe^{3+} on the XFe = 0 line. (online version in colour)

4. Results and discussion

4.1. Overview of cationic substitutions occurring in low-*T* chlorites

Beyond the debate on whether one should consider the Fe^{3+} content or a possible smectitic contamination of some chlorite analyses (*e.g*. Jiang *et al*., 1994), several studies comparing chlorite compositions in the 100–350°C range and at high-*T* concur to establish a link between decreasing octahedral vacancies and increasing temperature (*e.g*. Cathelineau & Nieva, 1985; Hillier & Velde, 1991; Inoue *et al*., 2009). Such a comparison is shown in Fig. 3, where the compositional spaces of several series of diagenetic and metamorphic chlorites are represented in an R^{2+}–Si diagram. The data series were selected for their wide ranges of chlorite composition and formation temperature in order to be representative of the most complete *T*–composition field. The chlorites considered in Fig. 3 were extracted from the following contributions: Foster (1962); McDowell & Elders (1980); Cathelineau (1988); Laird (1988); Velde & Medhioub (1988); Hutcheon (1990); Bevins *et al*. (1991); Jahren & Aagaard (1992); Rahn *et al*. (1994); Schmidt *et al*. (1997); Mas *et al*. (2006); Koroknai *et al*. (2008); Bourdelle *et al*. (2013a); Vidal & Parra (2000).

The compositional spaces defined for metamorphic chlorites are plotted along or close to the amesite/Al-free chlorite line, representing full octahedral occupancy (mirrored by silicon counter-variation). These chlorite compositions correspond to different degrees of Tschermak substitution, and are restricted to a $1.5 < R^{3+} < 3.5$ range (apfu), with Si contents essentially less than 3 apfu (Fig. 3b). Diagenetic chlorite compositions exhibit an extension toward the pyrophyllite-gibbsite/Al-free chlorite line (Fig. 3a). This deviation indicates a contribution of di-trioctahedral exchange in addition to Tschermak substitution. In fact, the variations in chlorite composition observed for each set, corresponding to all compositions of chlorites coming from the same geologic field, draw

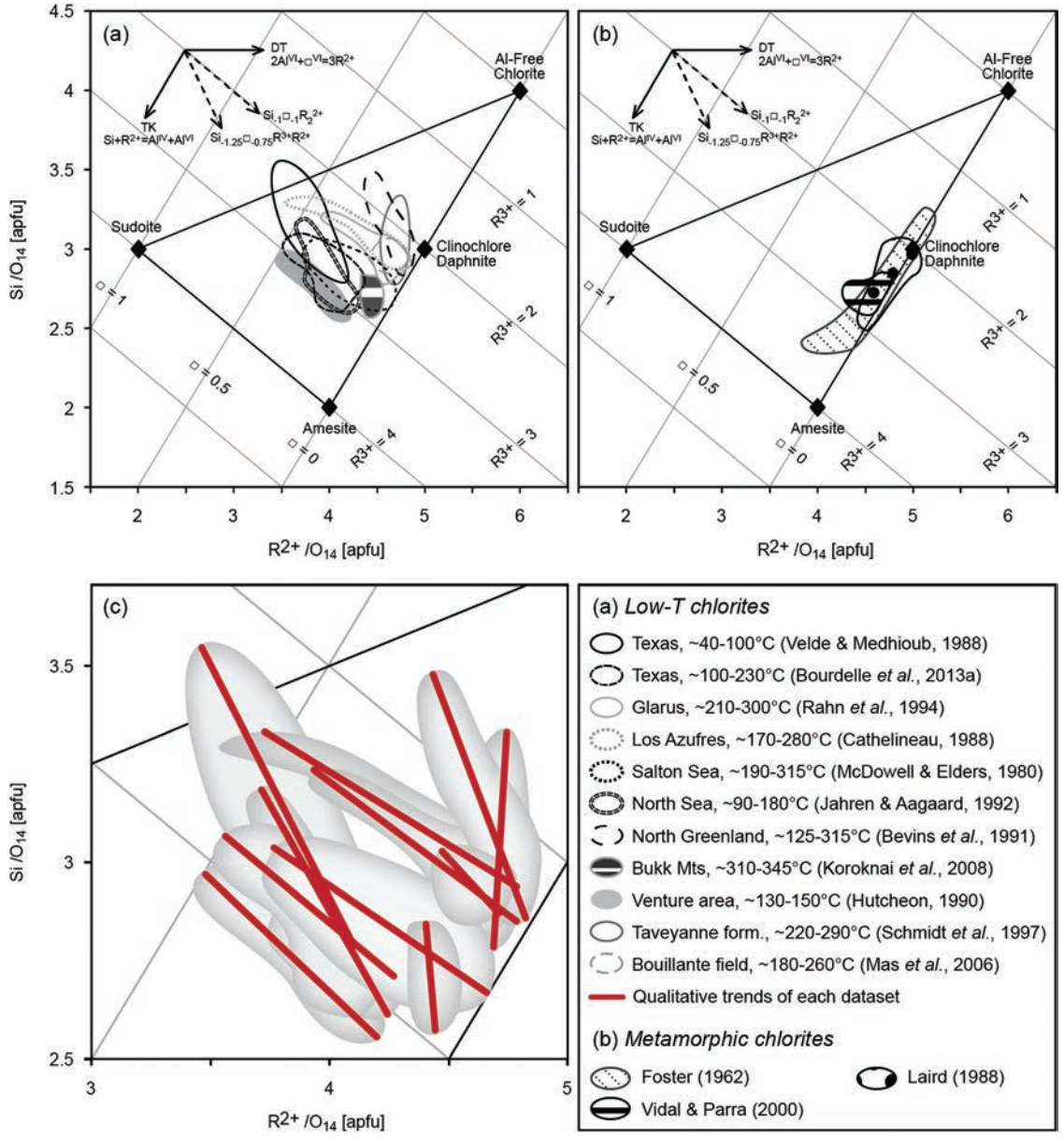

Fig. 3. Representation of compositional datasets of low-temperature (a) and metamorphic (b) chlorites from several geological settings in the R^{2+}–Si diagram of Wiewióra & Weiss (1990). All Fe is regarded as Fe^{2+}. For low-*T* chlorites, each set of compositional data was identified to a qualitative line (c). (online version in colour)

nearly parallel lines with respect to the line of a constant R^{3+} value (Fig. 3c). These parallels to the constant R^{3+} line underline the impact of a $Si_{-1}\square_{-1}R_2^{2+}$ exchange vector as a combination of Tschermak and di-trioctahedral substitutions in a 1/1 ratio (*i.e.*, $Si + \square + Al^{VI}$ substituted by $2R^{2+}+Al^{IV}$). In this case, the compositions can often be Si-rich/R^{2+}-poor compared to metamorphic chlorites, while the R^{3+} content is higher than 1.7 apfu and rarely exceeds 3 apfu (Fig. 3(a)). Low-*T* chlorite compositions do not plot on the same line, but on several sub-parallel lines at constant R^{3+} value, corresponding to different degrees of Tschermak exchange. However, some compositional sets are not strictly parallel to the $Si_{-1}\square_{-1}R_2^{2+}$ exchange vector, but seem to be more influenced by the Tschermak exchange. In fact, these datasets follow a combination of Tschermak and di-trioctahedral substitutions with a 5/3 ratio, given the $Si_{-1.25}\square_{-0.75}AlR^{2+}$ exchange vector (*i.e.*, $5Si + Al^{VI} + 3\square$ substituted by $5Al^{IV} + 4R^{2+}$).

Figure 4 assembles the chlorite compositional data plotted in Fig. 3 and their associated formation temperature, as determined by several independent methods. Several data series (Beaufort *et al.*, 1992; Xie *et al.*, 1997; Lopez-Munguira *et al.*, 2002; Potel, 2007) that were not selected initially were added to the datasets of Fig. 3 to complete Fig. 4; ~40 % of the chlorite compositional data considered here were not used for the calibration of the Bourdelle and Inoue thermometers. This representation shows that chlorites of very different

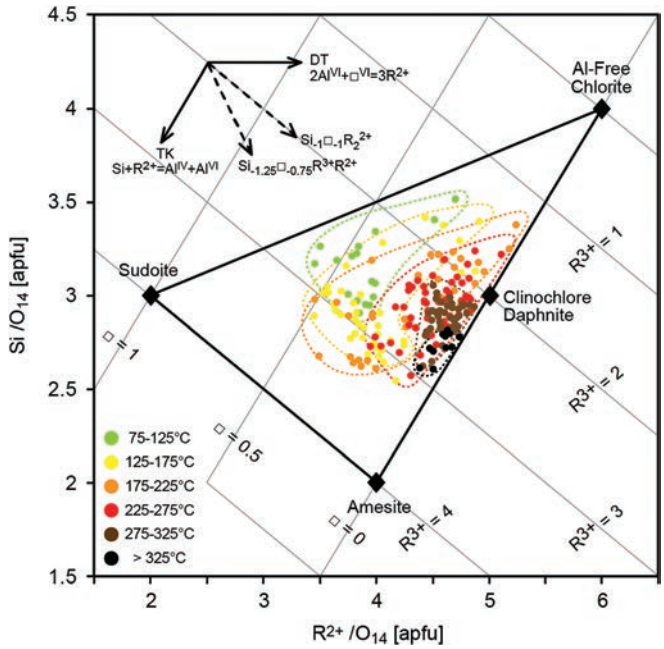

Fig. 4. Chemical composition of low-*T* chlorites plotted in the R^{2+}–Si diagram of Wiewióra & Weiss (1990). The data used are from the studies cited in Fig. 3(a), completed with the data of Beaufort *et al*. (1992); Xie *et al*. (1997); Lopez-Munguira *et al*. (2002) and Potel (2007). Data referring to T <75°C and/or outside the area defined by the selected end-members were excluded. All Fe is regarded as Fe^{2+}. The compositions were assembled according to their temperature of formation, which was determined by each author using several independent methods. (online version in colour)

compositions can be linked to a single temperature, and not on a random basis: the range of chlorite compositions for each defined temperature window (75–125°C, 125–175°C, 175–225°C, 225–275°C, 275–325°C, >325°C) can be assimilated to several lines sub-parallel to the Tschermak line, the resulting high-T isotherms being nearer to the clinochlore end-member than those for low temperatures (Fig. 4). Therefore, these resulting temperature domains are sub-perpendicular to the $Si_{-1}\square_{-1}R_2^{2+}$ and $Si_{-1.25}\square_{-0.75}AlR^{2+}$ vectors and to the lines of chlorite compositional variations defined for each geological setting (compare Fig. 3c and Fig. 4).

The $Si_{-1}\square_{-1}R_2^{2+}/Si_{-1.25}\square_{-0.75}AlR^{2+}$ exchange vectors are thus dependent on the temperature in the case of low-T chlorites, according to several lines (corresponding to variations in chlorite composition in each dataset) that are parallel to each other (as in Fig. 3c). These sub-parallel lines refer to the linear empirical thermometers established during the 1980's, which were limited to restricted chlorite compositional spaces. The thermometer of Cathelineau (1988) is therefore a specific case of the $Si_{-1}\square_{-1}R_2^{2+}$ exchange vector, *e.g*. for a given value of Tschermak substitution, and the equations proposed later should be graphically approximated by lines sub-parallel to it. The T-dependence of the $Si_{-1}\square_{-1}R_2^{2+}/Si_{-1.25}\square_{-0.75}AlR^{2+}$ exchanges also implies that octahedral vacancy decreases with increasing T. Therefore, the T–vacancies relationship is built into any geothermometer that was calibrated from databases including low-T chlorites. In the same way, variations in the chlorite + quartz log K remain negatively correlated with $1/T$, regardless of the assumption made as to the oxidation state of iron. This justifies calibrating a chlorite thermometer on one or the other assumption, that is, $Fe_{total} = Fe^{2+}$ or real Fe^{3+} values, whenever available. Admittedly, the evaluation of sudoite activity, which is directly related to vacancy content, can be incidentally biased by not considering the Fe^{3+} content, but this possible bias is built into the calibration.

4.2. Temperature–composition relationships from Bourdelle *et al*. (2013b) model

Temperatures were calculated using Bourdelle *et al*. (2013b) model for each point on the Si-R^{2+} diagram of Wiewióra & Weiss (1990) and used to define the compositional T-stability field in Fig. 5. The calculations were performed assuming quartz and water activities equal to 1, which seems reasonable for diagenetic conditions and in the case of quartz-bearing rocks.

In the compositional range of low-T chlorites ($1.5 < R^{3+} < 3.5$ apfu; Fig. 3), the calculated isotherms on Fig. 5 can be considered as sub-perpendicular to the $Si_{-1}\square_{-1}R_2^{2+}$ exchange vector in the upper part ($R^{3+} < 2.5$ apfu) and to the $Si_{-1.25}\square_{-0.75}AlR^{2+}$ exchange vector in the lower part ($2.5 < R^{3+}$ apfu). In fact, the equilibrium Eq. (4) involves sudoite and amesite as a Sud_{-3}/Am_{+3} exchange expressing

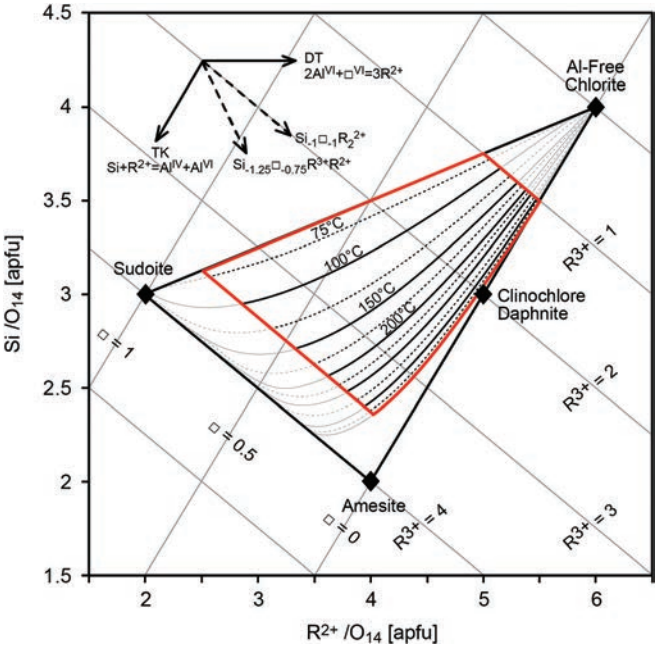

Fig. 5. Representation of isotherms (in 25°C steps) calculated with Bourdelle *et al*. (2013b) thermometer (Eq. 6) in a R^{2+}–Si diagram of Wiewióra & Weiss (1990). The area of optimal reliability for the thermometer is shown in red. The representative compositions are ideal compositions, devoid of Ti, Na, K and Ca. (online version in colour)

the $Si_{-1}\square_{-1}R_2^{2+}$ vector. Considering Al-free chlorite increases the Tschermak contribution: the equilibrium Eq. (4) is expressed by the $Si_{-1.25}\square_{-0.75}AlR^{2+}$ vector. The isotherms corresponding to the lowest temperatures (*i.e.*, $T <$ 75°C) are close to the sudoite/Al-free chlorite line, while those corresponding to higher temperatures (*i.e.*, $T >$ 300°C) are close to the amesite/Al-free chlorite line, where the compositions of metamorphic chlorites lie (Fig. 3b): there is therefore an increase in the estimated temperature when octahedral vacancy decreases. The shape of the isotherms also shows that, for a fixed temperature, several degrees of vacancy are possible (Fig. 5). This is compatible with the observation that chlorites crystallizing at the same temperature in rocks of different bulk compositions may have different compositions. Therefore, the degree of Tschermak exchange is linked predominantly to the geological context, *i.e*. to the lithology or local hydrothermal conditions.

The isotherms are close to each other in compositional spaces close to the Al-free chlorite or sudoite compositions. In fact, rather small compositional variations may induce rather large differences in the calculated temperatures when the chlorite composition is close to that of an end-member. This observation is probably verifiable for many geothermometers: the calculation using the log *K* of equilibrium, activities of end-members and cationic site partitioning are more reliable when the studied composition is far from that of the end-members. Fortunately, these kinds of ''extreme'' composition are rarely identified as natural low-*T* chlorites and the latter inconvenience is rarely encountered (see Fig. 3). Similarly, the temperature–composition relationships are somewhat speculative in the $\square$ <0.1 apfu/Si < 2.5 apfu window (*i.e*. where $T >$ 350°C) because it is outside the *T* range of applicability (T <350°C) of Bourdelle's thermometer. Again, low-*T* chlorites rarely have such compositions (Fig. 3). A gradual deviation of the isotherms can be also observed when $R^{3+} > 3.5$ apfu, *i.e*. when they become parallel to the sudoite/amesite line. This specific behaviour of isotherms has rather limited consequences, as most natural chlorite compositions have $R^{3+} < 3.5$ apfu (Fig. 3). From all these points, we can consider that the thermometer reliability is optimal in the compositional range $1 < R^{3+} < 3.5$ apfu.

Indeed, in the compositional space of most common diagenetic chlorites, the graphic isotherms predicted by Bourdelle *et al*. (2013b) geothermometer in the R^{2+}–Si diagram are in accordance with temperatures estimated from natural samples and constitute a useful tool for thermometric applications. Only a few extreme compositional domains that are rarely seen in nature are characterized by some *T*-prediction difficulties.

4.3. Temperature–composition relationships from the Inoue *et al*. (2009) model

The predictions of chlorite composition made with Inoue's model (quadratic equation) from *T* are shown in the R^{2+}–Si diagram of Fig. 6, considering the activities of water and silica to be equal to 1.

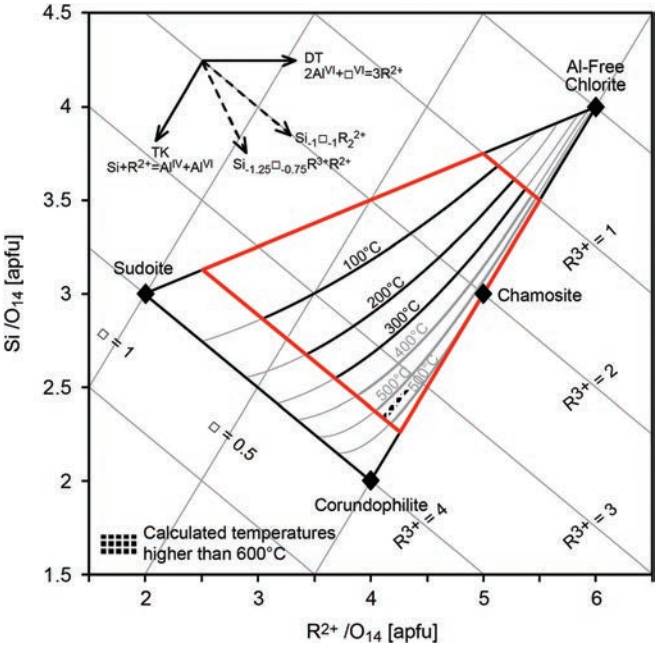

Fig. 6. Representation of isotherms (in 100°C steps) calculated with the quadratic equation (Eq. 7) of Inoue *et al*. (2009) thermometer in the R^{2+}–Si diagram of Wiewióra & Weiss (1990). The representative compositions are ideal compositions, devoid of Ti, Na, K and Ca. (online version in colour)

The isotherms are grossly parallel to the Al-free chlorite/amesite line, similar to those calculated using Bourdelle's model (Fig. 6). In fact, the two models show very similar isotherm shapes with the exception of isotherms near the amesite/sudoite line. Thus, the regular increase in temperature along the $Si_{-1}\square_{-1}R_2^{2+}/Si_{-1.25}\square_{-0.75}AlR^{2+}$ exchange vectors is disturbed close to the amesite composition, leading to a decrease when the vacancy is close to 0. This is due to the quadratic formalism of Inoue's thermometer, reflecting a reversal of the log *K*–*T* relationship. Thus, in this particular domain, for two compositions with the same R^{2+} content but different Si contents, a similar temperature estimate is obtained, a case which is not possible using a linear function (Eq. 8).

Although the isotherm shape is analogous for the two thermometers (Figs 5 and 6), the temperature values calculated according to the different equations are not similar. Therefore, for a given temperature, the corresponding isotherm determined by the equation of Inoue *et al*. (2009) is above that predicted by the model of Bourdelle *et al*. (2013b), *i.e*., closer to the Al-free chlorite/sudoite line. In fact, for a fixed *T* and Si content, the equations of Inoue predict R^{2+}-poorer/vacancy-richer compositions than the equation of Bourdelle. This divergence is due to the difference in the consideration of iron valence (see section 3.1): starting at an isotherm determined using Bourdelle's model, a portion of the iron should be considered as ferric in order to reach the equivalent isotherm using Inoue's model. This difference in how Fe^{3+} is considered between the two models implies a shift of reference frame, but does not preclude obtaining consistent (equivalent) temperature

estimates. This also justifies the calculation with Inoue's model of several isotherms with $T > 250$°C, even though Inoue *et al*. (2009) specified an upper limit of 250°C for the application of their model: these high-*T* isotherms refer to pure ferrous compositions. The convergence of the two models can give an approximation of the ferric iron content (except when $R^{3+} > 3.5$ apfu). The very low-*T* domain ($T < 150$°C) constitutes an exception because, for fixed Si and R^{2+} contents, the temperature calculated by Inoue's model is lower than the one given by Bourdelle's linear equation. In fact, the consideration of Fe^{3+} content coupled to the quadratic nature of the thermometer leads to an increase in the estimated temperature for very-low-*T* compositions.

5. Conclusion

In accordance with previous observations (*e.g*. Hillier & Velde, 1991; Inoue *et al*. 2009), a comparison of several data sets of chlorite compositions shows the coupled role of the Tschermak and di-trioctahedral substitutions in describing natural low-*T* chlorite compositions, and confirms the *T*-dependency of the $Si_{-1}\square_{-1}R_2^{2+}$, or close to it, exchange vector. The sub-perpendicular crossing of the compositional variations in chlorite for each geological setting with the isotherms allows the empirical thermometers to be reconciled with the temperature estimates given by the thermodynamic models. Practically, the use of the proposed *T*–composition diagram allows one to estimate the chlorite formation temperature from a single graphical plot of Si and R^{2+} contents, without calculations or thermodynamic parameters, and, on the other hand, to predict all chlorite compositions in equilibrium at fixed *T* for low-pressure quartz-bearing rocks. Therefore, the new *T*–R^{2+}–Si diagram proposed in this work (Appendix S3) provides a very practical tool for thermometric purposes within the given reliability range.

Acknowledgements: The discussions and comments of the journal editor Patrick Cordier, of the associate editor and of two anonymous reviewers are gratefully acknowledged. Thanks are also extended to Teddy Parra for his scientific help and to Olivier Beyssac and Christian Chopin for their support.

References

Bailey, S.W. (1988): Chlorites: structures and crystal chemistry. *in* ''Hydrous Phyllosilicates (Exclusive of Micas)'', S.W. Bailey, ed. *Rev. Mineral*., **19**, Mineralogical Society of America, Washington, 347–403.

Beaufort, D., Patrier, P., Meunier, A., Ottaviani, M.M. (1992): Chemical variations in assemblages including epidote and/or chlorite in the fossil hydrothermal system of Saint Martin (Lesser Antilles). *J. Volcanol. Geoth. Res.*, **51**, 95–114.

Bevins, R.E., Robinson, D., Rowbotham, G. (1991): Compositional variations in mafic phyllosilicates from regional low-grade metabasites and application of the chlorite geothermometer. *J. Metamorphic Geol.*, **9**, 711–721.

Bourdelle, F. (2011): Thermobarométrie des phyllosilicates dans les séries naturelles : conditions de la diagenése et du métamorphisme de bas degré. Ph.D. thesis, University Paris-Sud, Orsay, 318 p.

Bourdelle, F., Parra, T., Beyssac, O., Chopin, C., Vidal, O. (2013a): Clay minerals as geo-thermometer: A comparative study based on high spatial analyses of illite and chlorite in Gulf Coast sandstones (Texas, U.S.A. *Am. Mineral.*, **98**, 914–926.

Bourdelle, F., Parra, T., Chopin, C., Beyssac, O. (2013b): A new chlorite geothermometer for diagenetic to low-grade metamorphic conditions. *Contrib. Mineral. Petrol*., **165**, 723–735.

Bourdelle, F., Benzerara, K., Beyssac, O., Cosmidis, J., Neuville, D.R., Brown, G.E, Jr, Paineau, E. (2013c): Quantification of the ferric/ferrous iron ratio in silicates by scanning transmission X-ray microscopy at the Fe $L_{2,3}$ edges. *Contrib. Mineral. Petrol.*, **166**, 423–434.

Cathelineau, M. (1988): Cation site occupancy in chlorites and illites as a function of temperature. *Clay Miner.*, **23**, 471–485.

Cathelineau, M. & Nieva, D. (1985): A chlorite solid solution geothermometer. The Los Azufres (Mexico) geothermal system. *Contrib. Mineral. Petrol.*, **91**, 235–244.

de Caritat, P., Hutcheon, I., Walshe, J.L. (1993): Chlorite geothermometry: a review. *Clays Clay Miner.*, **41**, 219–239.

Foster, M.D. (1962): Interpretation of the composition and a classification of the chlorites. *U.S.G.S. Prof. Paper*, 414-A, 33 p.

Ganne, J., de Andrade, V., Weinberg, R.F., Vidal, O., Dubacq, B., Kagambega, N., Naba, S., Baratoux, L., Jessell, M., Allibon, J. (2012): Modern-style plate subduction preserved in the Palaeoproterozoic West African craton. *Nature Geosci.*, **5**, 60–65.

Grosch, E.G., Vidal, O., Abu-Alam, T., McLoughlin, N. (2012): P-T constraints on the metamorphic evolution of the paleoarchean Kromberg type-section, Barberton Greenstone Belt, South Africa. *J. Petrol.*, **53**, 513–545.

Harbi, H.M., Surour, A.A., Davidson, G.J. (2014): Genesis of Neoproterozoic Au-bearing volcanogenic sulfides and quartz veins in the Ar Rjum goldfield, Saudi Arabia. *Ore Geol. Rev.*, **58**, 110–125.

Hillier, S. & Velde, B. (1991): Octahedral occupancy and the chemical-composition of diagenetic (low-temperature) chlorites. *Clay Miner.*, **26**, 149–168.

Hutcheon, I. (1990): Clay carbonate reactions in the Venture area, Scotian Shelf, Nova Scotia, Canada. *The Geochemical Society, Special Publication*, **2**, 199–212.

Inoue, A., Meunier, A., Patrier-Mas, P., Rigault, C., Beaufort, D., Vieillard, P. (2009): Application of chemical geothermometry to low-temperature trioctahedral chlorites. *Clays Clay Miner.*, **57**, 371–382.

Inoue, A., Kurokawa, K., Hatta, T. (2010): Application of chlorite geothermometry to hydrothermal alteration in Toyoha geothermal system, Southwestern Hokkaido, Japan. *Resour. Geol.*, **60**, 52–70.

Jahren, J.S. & Aagaard, P. (1992): Diagenetic illite-chlorite assemblages in arenites.1. Chemical evolution. *Clays Clay Miner.*, **40**, 540–546.

Jiang, W.T., Peacor, D.R., Buseck, P.R. (1994): Chlorite geothermometry? - Contamination and apparent octahedral vacancies. *Clays Clay Miner.*, **42**, 593–605.

Jowett, E.C. (1991): Fitting iron and magnesium into the hydrothermal chlorite geothermometer. GAC/MAC/SEG Joint annual meeting, 16, Toronto, Canada, GAC/MAC/SEG.

Kameda, J., Ujiie, K., Yamaguchi, A., Kimura, G. (2011): Smectite to chlorite conversion by frictional heating along a subduction thrust. *Earth Planet. Sc. Lett.*, **305**, 161–170.

Kameda, J., Hina, S., Kobayashi, K., Yamaguchi, A., Hamada, Y., Yamamoto, Y., Hamahashi, M., Kimura, G. (2012): Silica diagenesis and its effect on interplate seismicity in cold subduction zones. *Earth Planet. Sc. Lett.*, **317**, 136–144.

Koroknai, B., Arkai, P., Horvath, P., Balogh, K. (2008): Anatomy of a transitional brittle-ductile shear zone developed in a low-T meta-andesite tuff: A microstructural, petrological and geochronological case study from the Bukk Mts. (NE Hungary). *J. Struct. Geol.*, **30**, 159–176.

Kranidiotis, P. & McLean, W.H. (1987): Systematics of chlorite alternation at the Phelps Dodge massive sulfide deposit, Matagami, Quebec. *Econ. Geol.*, **82**, 1898–1911.

Laird, J. (1988): Chlorites: metamorphic petrology. *in* ''Hydrous Phyllosilicates (Exclusive of Micas)'', S.W. Bailey, ed. **19**, Mineralogical Society of America, Washington D.C, 405–453.

Lanari, P., Wagner, T., Vidal, O. (2014): A thermodynamic model for di-trioctahedral chlorite from experimental and natural data in the system MgO–FeO–Al_2O_3–SiO_2–H_2O: applications to P–T sections and geothermometry. *Contrib. Mineral. Petrol.*, **167**, 968–xxx.

Lopez-Munguira, A., Nieto, F., Morata, D. (2002): Chlorite composition and geothermometry: a comparative HRTEM/AEM-EMPA-XRD study of Cambrian basic lavas from the Ossa Morena Zone, SW Spain. *Clay Miner.*, **37**, 267–281.

Mas, A., Guisseau, D., Mas, P.P., Beaufort, D., Genter, A., Sanjuan, B., Girard, J.P. (2006): Clay minerals related to the hydrothermal activity of the Bouillante geothermal field (Guadeloupe). *J. Volcanol. Geoth. Res.*, **158**, 380–400.

McDowell, S.D. & Elders, W.A. (1980): Authigenic layer silicate minerals in borehole Elmore 1, Salton Sea geothermal field, California, USA. *Contrib. Mineral. Petrol.*, **74**, 293–310.

Potel, S. (2007): Very low-grade metamorphic study in the pre-Late Cretaceous terranes of New Caledonia (southwest Pacific Ocean). *Island Arc*, **16**, 291–305.

Rahn, M., Mullis, J., Erdelbrock, K., Frey, M. (1994): Very low-grade metamorphism of the Taveyanne Greywacke, Glarus Alps, Switzerland. *J. Metamorphic Geol.*, **12**, 625–641.

Schmidt, D., Schmidt, S.T., Mullis, J., Mahlmann, R.F., Frey, M. (1997): Very low grade metamorphism of the Taveyanne formation of western Switzerland. *Contrib. Mineral. Petrol.*, **129**, 385–403.

Velde, B. & Medhioub, M. (1988): Approach to chemical equilibrium in diagenetic chlorites. *Contrib. Mineral. Petrol.*, **98**, 122–127.

Vidal, O. & Parra, T. (2000): Exhumation paths of high-pressure metapelites obtained from local equilibria for chlorite-phengite assemblages. *Geol. J.*, **35**, 139–161.

Vidal, O., Parra, T., Trotet, F. (2001): A thermodynamic model for Fe-Mg aluminous chlorite using data from phase equilibrium experiments and natural pelitic assemblages in the 100 degrees to 600 °C, 1 to 25 kb range. *Am. J. Sci.*, **301**, 557–592.

Vidal, O., Parra, T., Vieillard, P. (2005): Thermodynamic properties of the Tschermak solid solution in Fe-chlorite: Application to natural examples and possible role of oxidation. *Am. Mineral.*, **90**, 347–358.

Vidal, O., de Andrade, V., Lewin, E., Munoz, M., Parra, T., Pascarelli, S. (2006): P-T-deformation-Fe^{3+}/Fe^{2+} mapping at the thin section scale and comparison with XANES mapping: application to a garnet-bearing metapelite from the Sambagawa metamorphic belt (Japan). *J. Metamorphic Geol.*, **24**, 669–683.

Walshe, J.L. (1986): A six-component chlorite solid solution model and the conditions of chlorite formation in hydrothermal and geothermal systems. *Econ. Geol.*, **81**, 681–703.

Wiewiora, A. & Weiss, Z. (1990): Crystallochemical classifications of phyllosilicates based on the unified system of projection of chemical composition: II The chlorite group. *Clay Miner.*, **25**, 83–92.

Xie, X.G., Byerly, G.R., Ferrell, R.E. (1997): IIb trioctahedral chlorite from the Barberton greenstone belt: Crystal structure and rock composition constraints with implications to geothermometry. *Contrib. Mineral. Petrol.*, **126**, 275–291.

Yoneda, T. & Mokko, H. (2013): Significance of the mineralogical properties of phyllosilicate as an indicator in the exploration of ore deposits. Asean++2013 Moving Forward. ID 49, 1–6.

Zang, W. & Fyfe, W.S. (1995): Chloritization of the hydrothermally altered bedrock at the Igarape-Bahia gold deposit, Carajas, Brazil. *Miner. Deposita.*, **30**, 30–38.

Received 26 January 2015
Modified version received 19 May 2015
Accepted 22 May 2015